J. Fluid Mech. (1996), *vol.* 308, *pp.* 341–361

Permeability of three-dimensional models of fibrous porous media

By J. J. L. HIGDON AND G. D. FORD
Department of Chemical Engineering, University of Illinois, Urbana, IL 61801-3791, USA

(Received 14 October 1994 and in revised form 22 September 1995)

Viscous flow through three-dimensional models of fibrous porous media is analysed. The periodic models are based on ordered networks of cylindrical fibres on regular cubic lattices. Numerical solutions are obtained using the spectral boundary element method introduced by Muldowney & Higdon (1995). Results are presented for solid volume fractions ranging from extreme dilution to near the maximum volume fraction for permeable media. Theoretical estimates are derived using slender-body theory and lubrication approximations in the appropriate asymptotic regimes. Comparisons are made with model predictions based on properties of two-dimensional media (Jackson & James 1986), and with results for disordered dispersions of prolate spheroids (Claeys & Brady 1993*b*).

1. Introduction

Fluid flow through porous media plays an important role in a variety of engineering systems. In these applications, the porous materials may generally be divided into two classes: granular media and fibrous media. Granular media are composed of compact grains bound together to form a continuous solid matrix with a void space characterized by large open pores connected by networks of narrow constrictions. Common examples include rock formations in petroleum reservoirs, catalyst particles and packed beds employed in reactors and mass transfer operations Fibrous media may be composed of individual rod like particles or a complicated mesh of curving, intertwining fibres. Common examples of fibrous media include industrial filters, biological tissues, certain polymer membranes and many materials produced in the pulp and paper industry. In addition to these direct applications, fibrous porous media are of interest, because their properties are closely related to those of fibrous suspensions and entangled polymer networks.

Owing to their prevalence in industrial applications, granular media have received most of the attention in theoretical studies of porous materials. Numerous three-dimensional models have been developed with rigorous analyses of transport processes involving viscous flow, electrical conductivity, elastic deformation and acoustic wave propagation. A survey of these efforts has been given by Larson & Higdon (1989) and by Chapman & Higdon (1992, 1994). A comprehensive review of the literature on fibrous media has been conducted by Jackson & James (1986). These authors discuss a variety of theoretical models and present a large collection of experimental data for both natural and synthetic fibrous media. In contrast to granular media, Jackson & James find no rigorous analysis for any three-dimensional model of fibrous porous media. They give an extensive review of the models for two-dimensional media, divided into two categories: (i) flow aligned with arrays of parallel rods and (ii) flow normal to arrays of parallel rods. In the first category, Sparrow & Loeffler (1959) presented an

analysis for square and hexagonal lattices of circular cylinders valid at all concentrations. Drummond & Tahir (1984) repeated these calculations and developed an asymptotic expression for the permeability at small solids concentrations. Larson & Higdon (1986) extended the model to include a variety of lattices and inclusion shapes to investigate the properties of anisotropic materials. Larson & Higdon also employed these lattice models to study the flow characteristics near the boundary of a porous material.

The first rigorous analysis of flow normal to lattices of cylinders was presented by Hasimoto (1959) for square lattices at dilute concentrations. A later study by Sangani & Acrivos (1982*a*) extended the analysis to square and hexagonal lattices over the full range of concentrations. Drummond & Tahir (1984) obtained similar results using an independent method of computation. Larson & Higdon (1987) extended their earlier work to consider normal flow past anisotropic lattices and discussed normal flow in the boundary region of a finite porous medium. Based on this collection of work and the consistency of the results, we may conclude that the theory of two-dimensional ordered fibrous media has been well established. For disordered media, Howells (1974) developed a theory for dilute random arrays of parallel cylinders using an averaged-equation approach. Sangani & Yao (1988*a*, *b*) conducted numerical simulations of random arrays of parallel cylinders, finding good agreement with the predictions of Howells at low concentrations.

For three-dimensional media, there are only two studies cited by Jackson & James. The first, the 'swarm theory' of Spielman & Goren (1968), is a self-consistent field approximation. While this model was developed on a heuristic basis, it may be justified as the leading-order approximation in an averaged-equation approach for random media (Howells 1974). The second approach, by Jackson & James (1982) estimates the permeability of a cubic lattice by linear superposition of results for two-dimensional lattices parallel and normal to the flow direction. While this approach is valid in the asymptotic limit of small solids concentration ϕ, the first error term decays only as $(\ln \phi)^{-1}$. The models of Spielman & Goren and of Jackson & James yield similar predictions for the permeability and both are consistent with the experimental data. Unfortunately, it is difficult to assess the precision of these two models, because there is an order of magnitude of scatter in the experimental data. For disordered fibrous media, there have been no rigorous three-dimensional studies in the non-dilute regime. A recent study by Claeys & Brady (1993*a–c*) however does provide some insight into such media. These authors used the method of Stokesian dynamics to study transport properties of random dispersions of spheroids. While the dispersed solid phase is not directly equivalent to a fibrous porous medium, the permeability results provide an interesting comparison for our results on model fibrous media.

In the present effort, we present a rigorous numerical analysis of flow through three-dimensional models of ordered fibrous porous media. We consider cubic lattices of intersecting circular fibres and compute the permeability across the entire range of concentration. In addition to the numerical results, we provide theoretical predictions based on slender-body theory and lubrication theory for the low and high concentration limits respectively. Our goals are (i) to present accurate permeability results for a well-characterized model of a three-dimensional fibrous medium, (ii) to assess the accuracy range of the asymptotic theories, (iii) to compare this model with results for disordered media (Claeys & Bray 1993*a–c*) and with simpler models based on two-dimensional results (Jackson & James 1982). By extension, this last comparison provides a correlation with the wide range of experimental data reviewed by Jackson & James.

2. Formulation

Consider a fibrous porous medium composed of straight cylindrical fibres on periodic cubic lattices. We define a periodic unit cell as a cube of side $2b$ and hereafter render all lengths dimensionless with respect to b. The boundaries of the unit cell are then defined as the planes $x = \pm 1$, $y = \pm 1$, $z = \pm 1$. The base vectors s_i and internodal distances d for the three regular cubic lattices are defined as

(i) simple cubic (SC)

$$s_1 = (1,0,0), \quad s_2 = (0,1,0), \quad s_3 = (0,0,1), \quad d = 1; \tag{1}$$

(ii) body-centred cubic (BCC)

$$s_1 = (1,1,-1), \quad s_2 = (-1,1,1), \quad s_3 = (1,-1,1), \quad d = \sqrt{3}; \tag{2}$$

(iii) face-centred cubic (FCC)

$$s_1 = (1,1,0), \quad s_2 = (0,1,1), \quad s_3 = (1,0,1), \quad d = \sqrt{2}. \tag{3}$$

For each lattice, define a network of cylindrical fibres of radius a with axes extending from a lattice node to each of its nearest neighbours. For the SC lattice, each node connects six fibres with axes along directions $(\pm 1,0,0)$, $(0,\pm 1,0)$ and $(0,0,\pm 1)$. For the BCC lattice, there are eight nearest neighbours, yielding fibres along axes $(\pm 1,\pm 1,\pm 1)$. For the FCC lattice, there are twelve nearest neighbours with fibres along axes $(\pm 1,\pm 1,0)$, $(0,\pm 1,\pm 1)$ and $(\pm 1,0,\pm 1)$. Two views of the fibrous medium based on the FCC lattice are shown in figure 1.

For each lattice, the intersecting cylinders form a rigid solid matrix representing a fibrous porous medium. The maximum cylinder radius for which the medium is permeable occurs at $a = 1, 2^{-1/2}$ and $6^{-1/2}$ for the SC, BCC and FCC lattices respectively. The solid volume fractions ϕ and maximum values ϕ_{MAX} are given by

$$\left.\begin{array}{lll} \text{SC:} & \phi = \frac{3}{4}\pi a^2 - \sqrt{2}a^3, & \phi_{MAX} = 0.94198, \\ \text{BCC:} & \phi = \sqrt{3}\pi a^2 - 2\sqrt{6}a^3, & \phi_{MAX} = 0.98865, \\ \text{FCC:} & \phi = 3\sqrt{2}\pi a^2 - 8(1+\sqrt{2})a^3, & \phi_{MAX} = 0.90731. \end{array}\right\} \tag{4}$$

The term proportional to a^3 in each of these expressions is associated with the volume excluded by the intersection of the cylinders.

In the present paper, our goal is to calculate the permeability of a fibrous porous medium saturated with a viscous fluid flowing under the action of a mean pressure gradient G. Owing to the cubic symmetry, the permeability tensor is isotropic, and we may arbitrarily choose the pressure gradient aligned with the z-axis. Under conditions of low Reynolds number flow, the governing equations are the Stokes equation

$$-\nabla p + \mu \nabla^2 \boldsymbol{u} = 0 \tag{5}$$

and the continuity equation

$$\nabla \cdot \boldsymbol{u} = 0. \tag{6}$$

The no-slip boundary condition requires

$$\boldsymbol{u} = 0 \quad \text{on all cylinder surfaces.} \tag{7}$$

The conditions of periodicity require

$$\boldsymbol{u}(\boldsymbol{x}+\lambda) = \boldsymbol{u}(\boldsymbol{x}), \quad p(\boldsymbol{x}+\lambda) = p(\boldsymbol{x}) + G\lambda_z. \tag{8}$$

Here $\lambda = (2m_1, 2m_2, 2m_3)$ is any vector relating equivalent points in different unit cells, λ_z is the z component of λ, and m_1, m_2 and m_3 are integers.

The periodic boundary conditions (8) are valid for solid inclusions of any form. In the present circumstances, symmetry conditions may be exploited to simplify these

(*a*)

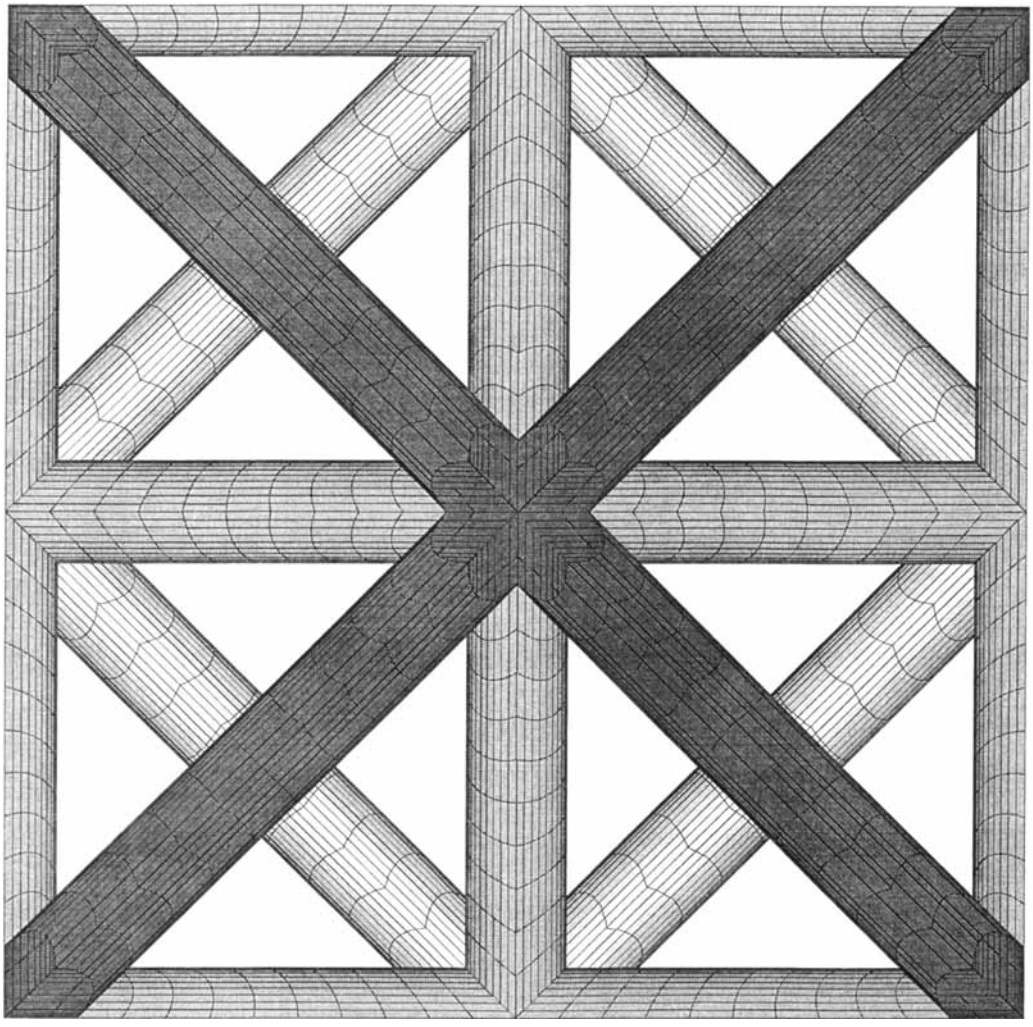

FIGURE 1 (*a*). For caption see facing page.

boundary conditions. Given a mean pressure gradient in the z-direction, the symmetry of the cubic lattices and the cylindrical fibres dictates that the velocity field has mirror symmetry about planes $x = 0$, $y = 0$, $x = y$ and antisymmetry about the plane $z = 0$. These constraints combined with periodicity require zero shear stress and normal velocity on the sides of the unit cell. On the top and bottom planes, the transverse velocity is zero, and the periodic part of the pressure field is constant. The resulting boundary conditions are

$$\left.\begin{aligned} u_x = 0, \quad f_y = 0, \quad f_z = 0 \quad \text{on} \quad x = \pm 1, \\ f_x = 0, \quad u_y = 0, \quad f_z = 0 \quad \text{on} \quad y = \pm 1, \\ u_x = 0, \quad u_y = 0, \quad f_z = G \quad \text{on} \quad z = \pm 1, \end{aligned}\right\} \tag{9}$$

where $\boldsymbol{f}$ is the surface stress vector defined by $\boldsymbol{f} = \sigma \cdot \boldsymbol{n}$.

Equations (5)–(9) constitute a well-posed boundary value problem for the three-dimensional Stokes equations. Numerous methods have been employed to solve these

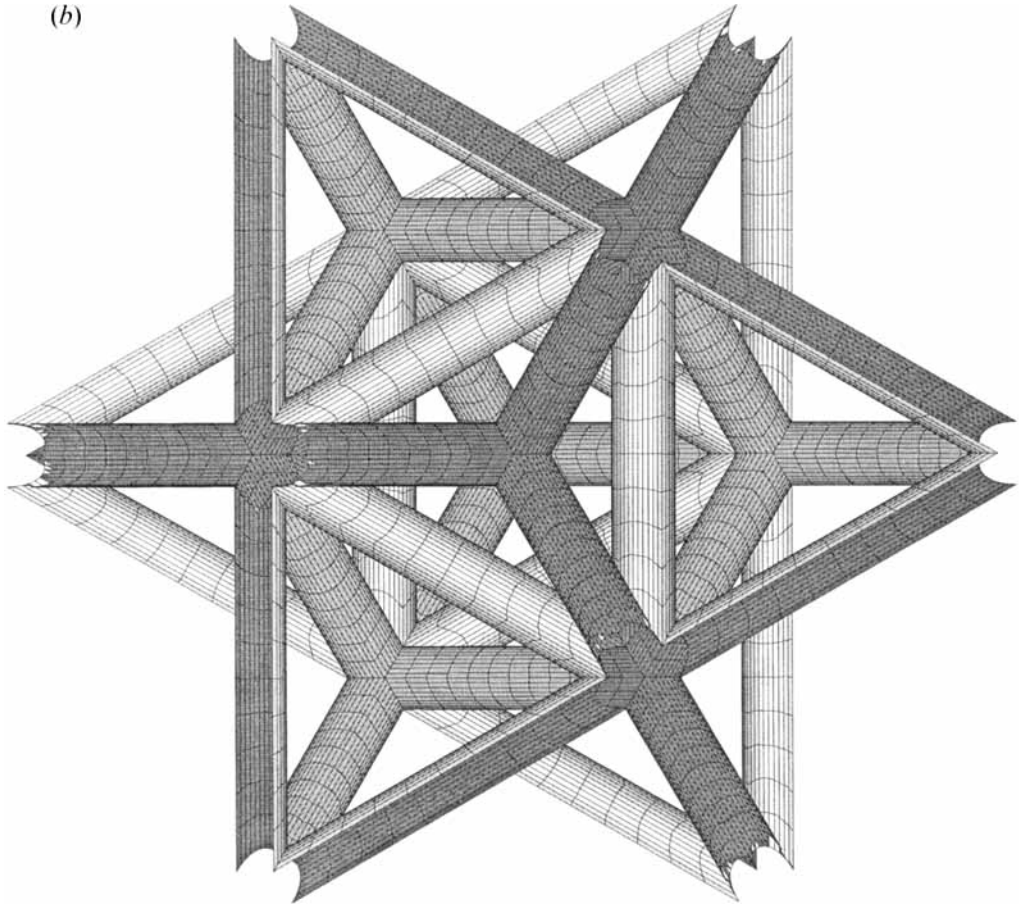

FIGURE 1. Three-dimensional views of fibrous medium based on an FCC lattice of circular cylinders. Lines represent contours of constant ξ or η, the parametric variables used to discretize the surface. Darker fibre segments represent the concave surface of a fibre as seen from the viewing direction. (*a*) Top view, view direction (0, 0, 1), (*b*) hexagonal plane view, view direction (1, 1, 1).

equations in previous studies of three-dimensional porous media. Zick & Homsy (1982) used a boundary integral approach with periodic Green's functions to solve for flow through lattices of spheres. Sangani & Acrivos (1982*b*) employed multipole expansion based on the periodic Green's function to attack the same problem. Larson & Higdon (1989) and Chapman & Higdon (1992) used multipole expansion based on the free-space Green's function to solve for flow through consolidated media with overlapping spheres. In the current effort, we have solved the Stokes equations using a version of the boundary integral method based on the spectral boundary element formulation developed by Muldowney & Higdon (1995). We give a brief account of the method here and refer the reader to Muldowney & Higdon (1995) for additional details regarding the computational implementation.

The boundary integral method for Stokes flow is based on the integral formula

$$u_i(\boldsymbol{x}_0) = \frac{1}{4\pi\mu}\int_{S_C+S_B} (S_{ij}f_j - \mu T_{ijk}\,u_j\,n_k)\,\mathrm{d}S, \tag{10}$$

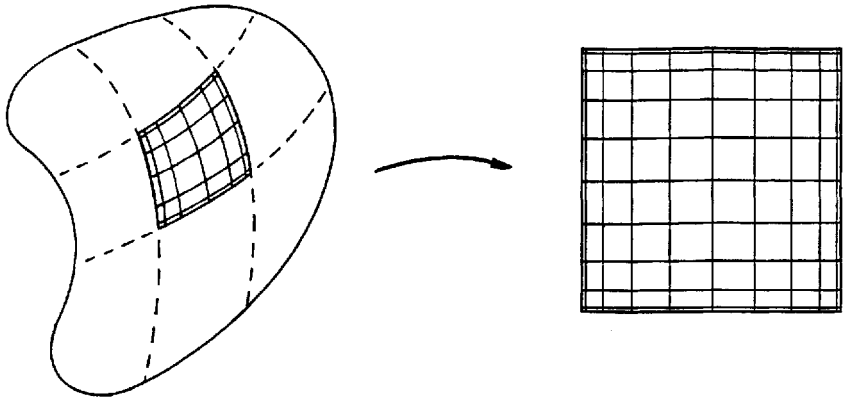

FIGURE 2. Mapping of spectral boundary element to square $[-1,1]\times[-1,1]$.

where $\boldsymbol{S}$ and $\boldsymbol{T}$ are defined by

$$S_{ij}(\hat{\boldsymbol{x}}) = \frac{\delta_{ij}}{|\hat{\boldsymbol{x}}|} + \frac{\hat{x}_i \hat{x}_j}{|\hat{\boldsymbol{x}}|^3}, \tag{11}$$

$$T_{ijk}(\hat{\boldsymbol{x}}) = -6\frac{\hat{x}_i \hat{x}_j \hat{x}_k}{|\hat{\boldsymbol{x}}|^5}; \tag{12}$$

$\hat{\boldsymbol{x}} = \boldsymbol{x} - \boldsymbol{x}_0$ and the unit normal vector $\boldsymbol{n}$ points into the fluid.

This integral formula expresses the velocity at a point $\boldsymbol{x}_0$ on the boundary of the fluid as an integral of the velocity and stress over the boundary. The surface of integration extends over the entire boundary of the fluid, which includes the cylinder surfaces S_C as well as the outer boundary of the unit cell S_B. A derivation of this equation may be found in recent monographs by Pozrikidis (1992) and Kim & Karilla (1991). When combined with the appropriate boundary conditions (7) and (9), equation (10) yields a Fredholm integral equation for the unknown velocities and stresses on the boundary surface.

In this paper, we solve the boundary integral equations using the spectral boundary element method. Let the boundary surface be divided into a collection of N_E curvilinear quadrilateral surface elements as illustrated in figure 2. On each element, the actual geometry is mapped onto a square $[-1,1]^2$ in terms of parametric variables ξ and η. All variables including the geometry $\boldsymbol{x}$ and the physical variables $\boldsymbol{u}, \boldsymbol{f}$ are discretized as Lagrangian interpolants in terms of these parametric variables. The base points (ξ_i, η_j) for the interpolations are chosen as the zeros of Legendre polynomials leading to interpolants which are equivalent to orthogonal polynomials. We define a set of N_G collocation points for the geometry and N_B collocation points as a basis for the physical variables. There is no requirement that the order of the geometry discretization match that of physical variables; however, this choice does simplify the programming effort.

With collocation points specified, the position of any point along the surface is expressed as a Lagrangian interpolant with respect to ξ and η; that is

$$\boldsymbol{x}(\xi,\eta) = \sum_{i=1}^{N_G}\sum_{j=1}^{N_G} \boldsymbol{x}(\xi_i,\eta_j)\, h_i(\xi)\, h_j(\eta), \tag{13}$$

where h_i is the (N_G-1)-order Lagrangian interpolant polynomial defined by $h_i(\xi_j) = \delta_{ij}$.

By a similar process, the physical variables $\boldsymbol{u}$ and $\boldsymbol{f}$ are defined at all points on the boundary as interpolants using the values at the basis collocation points

$$\boldsymbol{u}(\xi, \eta) = \sum_{i=1}^{N_B} \sum_{j=1}^{N_B} \boldsymbol{u}(\xi_i, \eta_j)\, h_i(\xi), h_j(\eta), \tag{14}$$

where h_i is the $(N_B - 1)$-order Lagrangian interpolant polynomial defined by $h_i(\xi_j) = \delta_{ij}$.

With the discretization of the geometry and physical variables completed, we substitute into the boundary integral formula (10), and require that the integral equation be satisfied at the discrete set of basis collocation points $\boldsymbol{x}(\xi_i, \eta_j)$, $i = 1, N_B$, $j = 1, N_B$. The discrete form of the integral equation yields a linear system of $3N_E N_B^2$ algebraic equations

$$\boldsymbol{u} = \boldsymbol{A}\boldsymbol{f} + \boldsymbol{B}\boldsymbol{u}. \tag{15}$$

These equations, combined with the boundary data at the $N_E N_B^2$ basis points, yields a consistent set of $3N_E N_B^2$ equations in $3N_E N_B^2$ unknowns.

The matrices $\boldsymbol{A}$ and $\boldsymbol{B}$ in the discrete system are defined as integrals of the kernels and basis functions over the collection of surface elements, Owing to the singularity in the kernels $\boldsymbol{S}$ and $\boldsymbol{T}$, special care must be taken to ensure the accurate numerical evaluation of these integrals. Muldowney & Higdon (1995) give a detailed description of the mapped Gaussian quadratures employed in evaluating these integrals. With the spectral element discretization described above, numerical convergence is achieved by increasing the order of the polynomial for a fixed set of elements. Convergence results demonstrating the accuracy of the method in the current application are described in §6 below.

3. Macroscopic properties

Using the techniques of the previous section, we may solve for the microscopic velocity field throughout the fluid domain. This velocity field may then be utilized to predict the macroscopic properties which characterize flow through a porous medium. For an isotropic medium, the mean fluid velocity $\boldsymbol{U}$ is related to the mean pressure gradient $\nabla \bar{p}$ though Darcy's law

$$\mu \boldsymbol{U} = -k \nabla \bar{p}, \tag{16}$$

where k is called the *permeability* of the medium.

To calculate k, we compute the volume flow rate Q as a surface integral over any horizontal plane through the unit cell, e.g.

$$Q = \int_{z=1} \boldsymbol{u} \cdot \boldsymbol{n}\, \mathrm{d}S. \tag{17}$$

The magnitude of the mean velocity is given by $U = Q/A$ where A is the area of the unit cell, equal to 4 in dimensionless units.

The permeability may be non-dimensionalized with respect to the fibre radius, yielding an expression

$$\frac{k}{a^2} = \frac{\mu Q}{GAa^2}, \tag{18}$$

where G is the magnitude of the mean pressure gradient.

For each lattice, k/a^2 is a function only of the volume fraction ϕ. It is important to emphasize that this is a physical quantity whose value depends upon the lattice type, but does not depend on the choice of unit cell. Thus one might employ the cubical unit cell specified here, or one of the regular polyhedra used by Chapman & Higdon (1992)

or Larson & Higdon (1989). The choice is dictated by computational convenience and does not affect the computed value of k/a^2. This result is related to the fact that there is no unique choice for the base vectors of a given periodic lattice.

While the permeability is the most common measure characterizing flow through a porous medium, certain authors prefer to calculate the mean force per unit length of fibre F. For our purposes, we define the fibre length L such that $\pi a^2 L = \phi V$ where ϕV is the total volume of solids in the unit cell. This yields the effective length of all fibres accounting for the region of cylinder overlap near the lattice nodes. With this definition, the force per unit length F is evaluated as

$$\frac{F}{\mu U} = \frac{GA\pi a^2}{\mu Q \phi} \tag{19}$$

and F is related to the dimensionless permeability by

$$\frac{F}{\mu U} = \frac{\pi}{\phi}\left(\frac{a^2}{k}\right). \tag{20}$$

Thus the dimensionless permeability k/a^2 and the dimensionless force $F/\mu U$ may each be determined solely as a function of volume fraction ϕ and of the lattice type.

4. Two-dimensional models

Before proceeding to the results of this paper, we summarize the principle results for two-dimensional media and for the simple model of Jackson & James for three-dimensional media. The permeability for flow parallel to lattices of circular cylinders has been calculated by Sparrow & Loeffler (1959) and by Drummond & Tahir (1984). The former authors present their results in graphical form, while the latter give expressions for the permeability for a square lattice

$$\frac{k}{a^2} = \frac{1}{4\phi}(-\ln\phi - 1.476 + 2\phi - \tfrac{1}{2}\phi^2 + O(\phi^4)) \tag{21}$$

and for a hexagonal lattice

$$\frac{k}{a^2} = \frac{1}{4\phi}(-\ln\phi - 1.498 + 2\phi - \tfrac{1}{2}\phi^2 + O(\phi^6)). \tag{22}$$

We define a hexagonal lattice as a collection of hexagonal unit cells covering the entire plane with a circular inclusion at the centre of each cell. This is called an equilateral triangle array by Drummond & Tahir.

We have recomputed the resistance for these lattices using the method of Sparrow & Loeffler and tabulate the results in table 1 for all concentrations from very dilute up to the maximum ϕ at which the cylinders make contact. These tabulated values are in excellent agreement with (21) and (22) for the smaller concentrations.

For flow normal to lattices of circular cylinders, Sangani & Acrivos (1982*a*) give asymptotic expressions for small ϕ and for ϕ near ϕ_{MAX} and give tabulations for intermediate values. Their results for small ϕ are

$$\frac{k}{a^2} = \frac{1}{8\phi}(-\ln\phi - 1.476 + 2\phi - 1.774\phi^2 + 4.076\phi^3 + O(\phi^4)) \tag{23}$$

for a square lattice, and

$$\frac{k}{a^2} = \frac{1}{8\phi}(-\ln\phi - 1.490 + 2\phi - \tfrac{1}{2}\phi^2 + O(\phi^4)) \tag{24}$$

	F_T		F_N	
ϕ	Square	Hexagonal	Square	Hexagonal
0.0001	1.625×10^0	1.629×10^0	3.250×10^0	3.259×10^0
0.0010	2.313×10^0	2.322×10^0	4.626×10^0	4.644×10^0
0.0100	3.991×10^0	4.018×10^0	7.982×10^0	8.036×10^0
0.0500	7.766×10^0	7.869×10^0	1.556×10^1	1.574×10^1
0.1000	1.230×10^1	1.257×10^1	2.483×10^1	2.513×10^1
0.2000	2.449×10^1	2.554×10^1	5.153×10^1	5.115×10^1
0.3000	4.453×10^1	4.806×10^1	1.029×10^2	9.679×10^1
0.4000	7.918×10^1	9.056×10^1	2.179×10^2	1.858×10^2
0.5000	1.413×10^2	1.781×10^2	5.325×10^2	3.822×10^2
0.6000	2.566×10^2	3.797×10^2	1.764×10^3	9.016×10^2
0.7000	4.765×10^2	9.204×10^2	1.352×10^4	2.770×10^3
0.7500	6.552×10^2	1.534×10^3	1.275×10^5	5.882×10^3
0.7854	8.246×10^2	2.280×10^3	∞	1.160×10^4
0.8000	—	2.710×10^3	—	1.623×10^4
0.8500	—	5.113×10^3	—	8.239×10^4
0.9069	—	1.148×10^4	—	∞

TABLE 1. Resistance force per unit length $F/\mu U$ for two-dimensional arrays of circular fibres as a function of volume fraction ϕ. Results are tabulated for flow tangential F_T and normal F_N to the cylinder axes.

for a hexagonal lattice.

The results for ϕ near ϕ_{MAX} are

$$\frac{k}{a^2} = \frac{2\sqrt{2}}{9\phi}\left(1-\left(\frac{\phi}{\phi_{MAX}}\right)^{1/2}\right)^{5/2} \tag{25}$$

for a square lattice, and

$$\frac{k}{a^2} = \frac{4\sqrt{2}}{27\phi}\left(1-\left(\frac{\phi}{\phi_{MAX}}\right)^{1/2}\right)^{5/2} \tag{26}$$

for a hexagonal lattice.

We have recomputed the resistance for normal flow past these lattices using a two-dimensional version of the spectral boundary element method. The results listed in table 1 are in excellent agreement with those of Sangani & Acrivos for all concentrations.

The two-dimensional results for permeability, or equivalently, force per unit length of fibre F may be employed to generate a simple model for three-dimensional media. Jackson & James (1982, 1986) employed such an approach to estimate the resistance of a simple cubic lattice of cylinders. They evaluated the tangential force at a concentration $\phi/3$ based on the number of axial fibres, and evaluated the normal force at $2\phi/3$ based on the number of transverse fibres. Their prediction yields

$$F_{JJ} = \tfrac{1}{3}F_T(\tfrac{1}{3}\phi) + \tfrac{2}{3}F_N(\tfrac{2}{3}\phi) \tag{27}$$

where F_T and F_N are the results for tangential and normal flow respectively.

With the two-dimensional results for square lattices, (21) and (23), used to compute F_T and F_N, the asymptotic prediction for the Jackson & James model is

$$\frac{F_{JJ}}{\mu U} \sim \frac{20\pi}{3}(-\ln\phi - 0.932)^{-1} + O\left(\frac{1}{(\ln\phi)^2}\right). \tag{28}$$

In the following section, we shall see that the functional form and the leading

coefficient are correct, and we shall compare the predictions of this model with a rigorous asymptotic theory.

5. Asymptotic theories

The resistance force on a periodic lattice of cylinders may be evaluated theoretically in two asymptotic limits: low concentration for which $a \to 0$ and high concentration for which $a \to a_{MAX}$. In the first case, the aspect ratio of the fibres a/d approaches zero and slender-body theory may be employed, while in the second, the gap between fibres approaches zero and lubrication estimates may be utilized. We begin with the analysis for slender-body theory.

The velocity field exterior to a body of arbitrary shape may be represented as a surface integral of Stokeslets $\boldsymbol{S}$ and their related stress $\boldsymbol{T}$ over the body surface as expressed in (10). For slender bodies whose radius a is much smaller than other length scales, this velocity may be approximated by a line distribution of Stokeslets and higher-order singularities along the body centreline (Johnson 1980). Consider a straight circular cylinder of radius a and length $d/2$ whose centreline lies on the line Γ_N. (Recall that our fibres are of length d; here we consider half of the fibre length.) Let the disturbance velocity induced by this slender body be represented by a distribution of Stokeslets $\boldsymbol{S}$ and dipoles $\boldsymbol{D}$ along the body axis

$$u_i = \int_{\Gamma_N} (S_{ij}\,\alpha_j + D_{ij}\,\beta_j)\,\mathrm{d}s, \tag{29}$$

where α and β are the Stokeslet and dipole strengths per unit length, $\mathrm{d}s$ is the differential arc length and $\boldsymbol{D}$ is the dipole singularity defined as

$$D_{ij}(\hat{\boldsymbol{x}}) = \frac{\delta_{ij}}{|\hat{\boldsymbol{x}}|^3} - \frac{3\hat{x}_i\,\hat{x}_j}{|\hat{\boldsymbol{x}}|^5}. \tag{30}$$

For a given point s_0 on the body axis Γ_N, one may evaluate the velocity (29) on the cylinder surface be employing inner and outer expansions of the integrand. The dipole strength β_j may be related to the force distribution α_j, and the integrals yield (Johnson 1980)

$$u_i(s_0) = J_{ij}(s_0)\,\alpha_j(s_0) + \int_{\Gamma_N} K_{ij}\,\alpha_j\,\mathrm{d}s, \tag{31}$$

where

$$J_{ij} = \delta_{ij}(2\mathscr{L}+1) + t_i\,t_j(2\mathscr{L}-3), \tag{32}$$

$$K_{ij} = S_{ij} - \frac{\delta_{ij}+t_i\,t_j}{|s_0-s|}, \tag{33}$$

and

$$\mathscr{L} = \ln\frac{d}{a} + \frac{1}{2}\ln\frac{4(s-s_1)\,(s_2-s)}{d^2}. \tag{34}$$

In these expressions $\boldsymbol{t}$ is the local unit tangent vector and s_1 and s_2 are the limits of integration along the fibre. Equations (31)–(34) are the Cartesian tensor form of Johnson's equation (33). For a fibre immersed in a velocity field $\boldsymbol{u}^\infty$, the no-slip boundary condition combined with (31) yields an integral equation for the force distribution α.

The expressions above represent the velocity on a single fibre induced by singularities along that fibre. For a periodic lattice of intersecting fibres, we focus on a given lattice node, and consider a collection of fibres Γ_M extending from that node toward each of

its nearest neighbours. With each fibre of length $d/2$, this collection constitutes the basic unit for the periodic lattice. The velocity at a point s_0 on fibre Γ_N may be written

$$u_i(s_0) = J_{ij}\,\alpha_{Nj}(s_0) + \int_{\Gamma_N} K_{ij}\,\alpha_{Nj}\,\mathrm{d}s + \sum_{M \neq N} \int_{\Gamma_M} S_{ij}\,\alpha_{Mj}\,\mathrm{d}s, \tag{35}$$

where α_{mj} is the force distribution on fibre Γ_M.

To extend this result to an infinite periodic lattice, we employ the periodic Green's function $\boldsymbol{S}^P$ as derived by Hasimoto (1959). Substituting $\boldsymbol{S}^P$ for $\boldsymbol{S}$ in (35) and in the definition of $\boldsymbol{K}$ in (33) yields the correct form for the disturbance velocity for all fibres of the periodic lattice.

For isolated fibres under the proper restrictions, Johnson has shown that the solution to the integral equation (31) determines the force distribution to within an error of $O(\epsilon^2)$ where ϵ is the ratio a/ℓ and ℓ is a characteristic length scale. The length ℓ is given by the minimum of the body length, the centreline radius of curvature and any characteristic length associated with $\boldsymbol{u}^\infty$. The $O(\epsilon^2)$ accuracy requires two conditions which are not met in the present application: (i) the ends of the fibres must be no blunter than those of an equivalent ellipsoid, and (ii) no segment along the body axis may pass close to another segment along the axis. The constant-radius cylinders and intersecting fibres of our model violate these assumptions. Under these conditions, the velocity represented by (35) yields an $O(1)$ error near the ends of each fibre which decays as $\ln(s^{-1})/\ln(\epsilon^{-1})$ as one moves a distance s from the end. The integrated effect on the solution for the force distribution α yields an error of $O(\epsilon)$ in the total force on a fibre. Thus, slender-body theory as described above yields an error of $O(a/d)$ for the force on the periodic cylinder lattices in our model fibrous medium.

There are two strategies for solving the integral equation represented by equation (35). In the first, one may choose a suitable discretization and obtain a numerical solution for the force distribution α. We have implemented this approach using a one-dimensional version of the spectral boundary element method with excellent results. A second approach is to use (35) as the basis of an iterative solution, yielding a series solution in inverse powers of $\ln(d/a)$. To pursue this alternative, we rearrange the equation, extracting the $\ln(d/a)$ term from the definition of $\mathscr{L}$ and write

$$\alpha_{Nk}(s_0) = \frac{1}{2\ln(d/a)}(\delta_{ki} - \tfrac{1}{2}t_k\,t_i)\Big\{u_i^\infty(s_0) - J'_{ij}\,\alpha_{Nj}(s_0) - \int_{\Gamma_N} K_{ij}^P\,\alpha_{Nj}\,\mathrm{d}s - \sum_{M \neq N}\int_{\Gamma_M} S_{ij}^P\,\alpha_{Mj}\,\mathrm{d}s\Big\}. \tag{36}$$

Here we have written $\boldsymbol{J}'$ to designate the modified expression with the $\ln(d/a)$ term extracted from $\mathscr{L}$. We have written $\boldsymbol{S}^P$ and $\boldsymbol{K}^P$ to emphasize that these kernels are based on the periodic Green's function.

Equation (36) is the equivalent of Johnson's (34). With an initial guess $\alpha = 0$ on the right-hand side, the left-hand side yields the leading-order solution for α, and successive application of this iteration yields a series solution in inverse powers of $\ln(d/a)$. A few comments concerning the numerical execution of this procedure are in order. First, the periodic Green's functions are evaluated by the Ewald summation technique described by Hasimoto. The integrals on the right-hand side of (36) are evaluated numerically using a combination of high-order Gaussian quadratures and variable mappings. These integrations require some care owing to the singularities in the kernels and the logarithmic singularity in the force distributions α at the fibre intersections.

n	SC	BCC	FCC
0	1	1	1
1	-1.527×10^{0}	-1.627×10^{0}	-2.694×10^{0}
2	-1.890×10^{0}	-2.733×10^{0}	-1.137×10^{1}
3	-7.759×10^{0}	-1.430×10^{1}	-1.028×10^{2}
4	-3.279×10^{1}	-7.858×10^{1}	-1.018×10^{3}
5	-1.424×10^{2}	-4.565×10^{2}	-1.084×10^{4}
6	-6.329×10^{2}	-2.798×10^{3}	-1.220×10^{5}
7	-2.867×10^{3}	-1.797×10^{4}	-1.427×10^{6}
8	-1.317×10^{4}	-1.199×10^{5}	-1.717×10^{7}
9	-6.104×10^{4}	-8.204×10^{5}	-2.104×10^{8}
10	-2.838×10^{5}	-5.718×10^{6}	-2.619×10^{9}
11	-1.315×10^{6}	-4.021×10^{7}	-3.289×10^{10}
12	-6.011×10^{6}	-2.832×10^{8}	-4.161×10^{11}
13	-2.660×10^{7}	-1.984×10^{9}	-5.292×10^{12}
14	-1.095×10^{8}	-1.369×10^{10}	-6.712×10^{13}

TABLE 2. Coefficients C_n for asymptotic expansions for $F/\mu U$ as defined in equation (39).

For each of the three lattices (SC, BCC, FCC), we have computed the first 15 terms in the asymptotic expansion. This yields an expression for the mean force/length on the fibres in the form

$$\frac{F}{\mu U}=\frac{10\pi}{3}\sum_{n=1}^{15}A_n(\ln(d/a))^{-n}. \tag{37}$$

In the interest of brevity, we do not present the coefficients A_n for these series; however, their values may be recovered from the coefficients in table 2 as described below.

In principle, the inclusion of a large number of terms in the asymptotic series might yield results of accuracy comparable to the direct numerical solution. In practice, we find that the radius of convergence of these series is limited by a singularity on the negative real axis. A Domb–Sykes plot or d'Alembert ratio test (see Van Dyke 1974) reveals the approximate location of the singularity and shows it to be a simple pole. As suggested by van Dyke, we map this singularity to $-\infty$ by introducing an Euler transformation, recasting the series as

$$\frac{F}{\mu U}=\frac{10\pi}{3}\sum_{n=1}^{15}B_n(\ln(d/a)+l_0)^{-n}, \tag{38}$$

where the constant l_0 takes the values 3.2, 6.13 and 12.7 for the SC, BCC and FCC lattices respectively. The coefficients B_n may be recovered from the coefficients in table 2 below.

While (38) yields improved convergence, the series coefficients now show that the nearest singularity is located on the positive real axis. This is a physical singularity corresponding to small aspect ratios where the slender-body approximation breaks down. This singularity, which is also a simple pole, may be extracted in a multiplicative fashion (Van Dyke 1974) to improve the convergence of the series. The result is

$$\frac{F}{\mu U}=\frac{10\pi}{3}\frac{1}{\ln(d/a)-l_1}\sum_{n=0}^{14}\frac{C_n}{(\ln(d/a)+l_0)^n}. \tag{39}$$

The constant l_1 is 2.0, 1.96, 2.21 for the SC, BCC and FCC lattices respectively. The coefficients C_n for each of the three lattices are presented in table 2.

To demonstrate the limits of the simple expansion (37) and the improved performance of the asymptotic series (38) and (39), we plot the force $F/\mu U$ as a

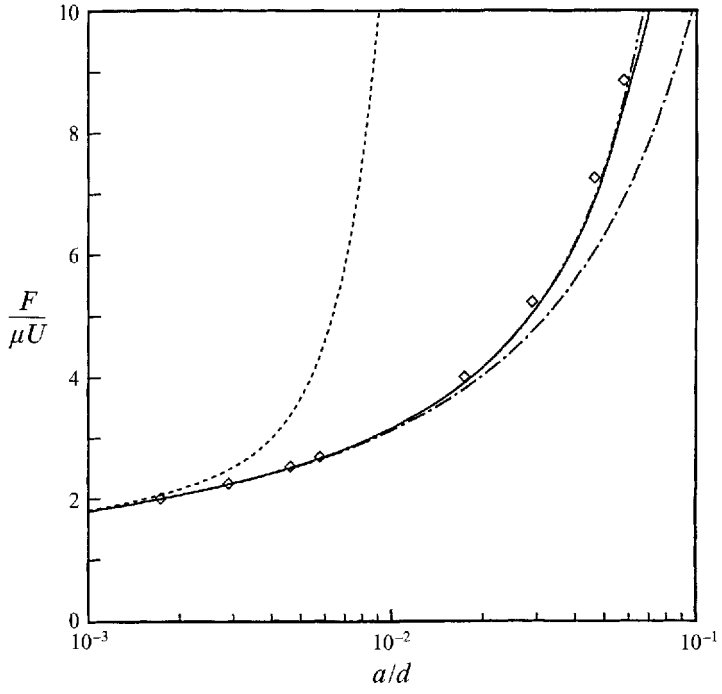

FIGURE 3. Resistance force per unit length $F/\mu U$ for a BCC fibre lattice as a function of solid fibre aspect ratio d/a. Curves are results from slender-body theory: ——, numerical solution; -----, asymptotic series (37); —·—, modified series (38); —··—, modified series (39). Symbols ◇ are spectral boundary element results for a BCC lattice.

function of a/d for each of these series and compare with the numerical solutions of the slender-body equations and the results of the full spectral element solution. Figure 3 shows the results for the BCC lattice. We observe that the simple expansion has a very limited range, departing from the numerical solution at a/d of order 3×10^{-3}. The extraction of the first singularity extends the useful range by an order of magnitude, and the final series (39) yields results which are indistinguishable from the numerical solution over the entire range. We note that both the asymptotic series (39) and the numerical solution for slender-body theory show excellent agreement with the spectral boundary element results up to $a/d = 0.08$, i.e. an aspect ratio of order 12:1. A detailed examination of the numerical results confirms the $O(a/d)$ accuracy of the slender-body integral equation (35). The qualitative behaviour of the SC and FCC results (not shown) is similar to that for the BCC case. The performance of the simpler series (37), (38) is closer to that of (39) for SC and is much worse for the FCC lattice. The final series (39) closely matches the numerical solution in all cases. A further comparison of these results with the three-dimensional spectral element results will be presented in §6.

As the concentration of the porous medium approaches its maximum value with $a \to a_{MAX}$, the pressure change in the medium is dominated by that occurring in narrow constrictions where the open cross-section reaches its minimum size. These constrictions form channels of simple cross-section (square for SC, BCC; equilateral triangle for FCC) whose size changes slowly compared to their length. In these circumstances, it is possible to predict the pressure change by employing a lubrication theory based on a straight channel with the same cross-section. This approach has been used previously by Larson & Higdon (1989) and Chapman & Higdon (1994) who provide details of the lubrication model.

The cross-section of the narrow channel in each fibre lattice may be characterized by a length scale ℓ which we define as the half-side for the square channel and as the radius of an inscribed circle for the triangular channel. The cross-sectional length scale is determined by the lattice geometry and may be expressed as

$$\ell = a_{MAX} - a + \kappa s^2, \tag{40}$$

where s is the arclength measured along the channel, and κ takes values $1/(2a)$, $2^{-1/2}/3$ and $1/(2a)$ for the SC, BCC and FCC lattices respectively.

With this geometry specification, it is straightforward to evaluate the pressure change along the channels as a function of volume flow rate, and hence to determine the permeability of the medium. For the unit cube specified in §2, the volume flow rate in each channel equals the total flow through the unit cell for the SC and BCC geometries. For the FCC geometry, the flow through each constriction is 1/8 the total flow, while the fluid passes through four constrictions in traversing the cell. In this latter case, the ratio $Q/\Delta p$ for the medium is thus twice that for a single channel. The lubrication results for the permeability are

$$\left.\begin{aligned} \text{SC:}\quad & \frac{k}{a^2} = 0.202\,50\,(a_{MAX}-a)^{7/2}a^{-5/2}, \\ \text{BCC:}\quad & \frac{k}{a^2} = 0.196\,63\,(a_{MAX}-a)^{7/2}a^{-2}, \\ \text{FCC:}\quad & \frac{k}{a^2} = 0.561\,38\,(a_{MAX}-a)^{7/2}a^{-5/2}. \end{aligned}\right\} \tag{41}$$

The scaling $k/a^2 \sim (a_{MAX}-a)^{7/2}$ in these lattices may be contrasted with that found by Sangani & Acrivos for the two-dimensional lattices $k/a^2 \sim (a_{MAX}-a)^{5/2}$. The difference lies in the fact that the limiting channel geometry in two dimensions is a pair of parallel plates of infinite width, in contrast to the square and triangular channels of the three-dimensional media.

In the following section, we shall compare the lubrication results with the three-dimensional spectral boundary element computations.

6. Results

Numerical solutions for the fluid velocity field and for the macroscopic parameters are computed using the spectral boundary element method as described in §2 above. For the SC lattices, we shift the unit cell to position the fibre nodes at the corners of the cube with the fibre axes along the edges of the unit cell. In this configuration, the domain is discretized with two spectral elements per quarter cylinder, and one element per cube face for a total of 30 elements. For certain cases with small fibre radius, the cube faces are divided into five elements yielding a total of 54 elements. For the BCC lattices, the discretization employs six elements on each of the eight cylinders, and five elements per cube face giving a total of 78 elements. For the FCC lattice, each full cylinder is divided into four elements and each cube face is divided into four elements. There are 12 full fibres radiating from the centre node, plus an additional collection of truncated fibres on the walls of the unit cell (see figure 1*a*). Thus there are the equivalent of 24 full fibres in the unit cell with a total of 120 elements.

For each lattice, the total number of unknowns $3N_B^2 N_E$ may be reduced 16-fold by exploiting the symmetry about the planes $x = 0$, $y = 0$, $x = y$ and $z = 0$. Thus a 6×6-

	SC			BCC			FCC		
a	0.01	0.50	0.95	0.01	0.40	0.65	0.01	0.20	0.35
N_B									
6	-2.4×10^{-3}	-1.4×10^{-3}	1.4×10^{-2}	4.0×10^{-3}	7.9×10^{-5}	7.4×10^{-2}	-6.2×10^{-3}	1.7×10^{-4}	8.8×10^{-3}
7	-1.2×10^{-3}	-2.8×10^{-4}	3.8×10^{-3}	2.4×10^{-3}	7.9×10^{-5}	8.9×10^{-3}	-3.4×10^{-3}	6.1×10^{-6}	-5.8×10^{-3}
8	-5.8×10^{-4}	-1.2×10^{-4}	2.3×10^{-4}	1.0×10^{-3}	-5.9×10^{-6}	-1.3×10^{-2}	-2.0×10^{-3}	-8.4×10^{-6}	6.6×10^{-4}
9	-2.0×10^{-4}	-1.4×10^{-5}	-1.0×10^{-4}	4.2×10^{-4}	-6.3×10^{-6}	1.1×10^{-3}	-4.7×10^{-4}	-2.7×10^{-6}	-1.2×10^{-4}
10	5.4653×10^{3}	7.8175×10^{2}	6.2833×10^{-6}	2.166×10^{3}	2.67190×10^{-2}	2.157×10^{-5}	8.080×10^{2}	1.01092×10^{-1}	3.4423×10^{-4}

TABLE 3. Convergence results for permeability of fibre lattices as a function of N_B, the number of basis points employed in the spectral boundary element discretization. The table shows the relative error in permeability for three values of fibre radius a on each lattice type, SC, BCC and FCC. The bottom row gives the computed value k/a^2 for $N_B = 10$.

order solution for the 30 element SC lattice leads to 207 unknowns, while the 10×10 solution on the FCC lattice yields approximately 2250 unknowns. All computations were performed on IBM RS/6000 workstations or an SGI Challenge parallel processor. Typical single processor times on the SGI Challenge ranged from 20 s for the 6×6 SC lattice to 120 s for a 6×6 BCC lattice to 1450 s for a 10×10 FCC computation. Multiprocessor runs decreased approximately linearly with the number of c.p.u.s. using up to eight processors. Computation times on an IBM RS6000/370 were roughly 40% to 50% of those on the single processor SGI.

We begin our discussion of the numerical results with a selection of test runs which demonstrate the convergence of the spectral boundary element algorithm. Table 3 lists the computed value of the dimensionless permeability k/a^2 as a function of the spectral polynomial order N_B. Convergence runs are shown for each of the three lattices with results for three radii corresponding to a slender fibre ($a = 0.01$), a fibre of moderate thickness and a fibre near the maximum radius for which the overlapping cylinders completely seal off the flow. The small fibres present a computational challenge because the spectral discretization must resolve the velocity dependence which approaches $\ln r$ for small radii. The large fibres present a challenge because the shear stress reaches large values in the narrow constrictions in the lubrication limit as the channels are pinched off. The intermediate radii present the least computational challenge. Despite these challenges, the spectral boundary element computations demonstrate excellent convergence in all cases with a maximum relative error of 1×10^{-3} for the BCC lattice and 5×10^{-4} for the SC and FCC cases.

The major numerical results of this paper are shown in table 4. This table presents the permeability k/a^2 and the dimensionless force $F/\mu L$ for each lattice over a range of fibre radii from the dilute limit to concentrations approaching the limit of zero permeability. Convergence tests have been conducted to confirm the precision of the results in all cases with an error of ± 1 in the last figure shown. An independent confirmation of the results is obtained by comparison with the permeability or resistance force predicted by the asymptotic theories of §5. Figure 4(*a*) shows the dimensionless force $F/\mu U$ plotted versus volume fraction ϕ for the three lattices. At small concentrations we show the predictions based on slender-body theory (39), while at high concentrations we plot the results of the lubrication approximation (41). Finally, we show the prediction of Jackson & James (27) using accurate numerical values for F_T and F_N. At low concentrations, we observe that all three lattices yield similar results for the resistance force. Slender-body theory shows good agreement with these results up to 5% for the SC lattice and up to 10% for the BCC and FCC cases. The limit of accuracy for slender-body theory is determined by the aspect ratio of the fibres. At the same aspect ratio, the latter two cases have a higher volume fraction, hence the slightly greater range of validity. The lubrication approximations show excellent agreement with the numerical results at high concentrations, and yield a good approximation down to approximately 75% to 80% of ϕ_{MAX}. The model of Jackson & James overpredicts the resistance by up to 25% at low concentration (around 1%) and shows best agreement in the range 10% to 20% volume fraction. Above this level, the model significantly underpredicts the resistance force. The results of Jackson & James are of interest because they provide a comparison with the large sample of experimental data reviewed by those authors. The experimental data covering volume fractions from 0 to 30% were well matched by the prediction of Jackson & James, and hence agree well with the current idealized models of fibrous media.

Turning our attention to the permeability, we plot k/a^2 versus volume fraction in figure 4(*b*). The results of this figure reflect the same behaviour as in figure 4(*a*), as one

	SC			BCC			FCC		
a	ϕ	k/a^2	$F/\mu U$	ϕ	k/a^2	$F/\mu U$	ϕ	k/a^2	$F/\mu U$
0.001	2.35×10^{-6}	8.550×10^{5}	1.560×10^{0}	5.44×10^{-6}	3.547×10^{5}	1.629×10^{0}	1.33×10^{-5}	1.372×10^{5}	1.721×10^{0}
0.003	2.12×10^{-5}	7.883×10^{4}	1.883×10^{0}	4.88×10^{-5}	3.216×10^{4}	2.000×10^{0}	1.19×10^{-4}	1.237×10^{4}	2.126×10^{0}
0.005	5.87×10^{-5}	2.563×10^{4}	2.087×10^{0}	1.35×10^{-4}	1.035×10^{4}	2.241×10^{0}	3.31×10^{-4}	3.947×10^{3}	2.406×10^{0}
0.008	1.50×10^{-4}	9.016×10^{3}	2.322×10^{0}	3.46×10^{-4}	3.597×10^{3}	2.526×10^{0}	8.43×10^{-4}	1.354×10^{3}	2.752×10^{0}
0.010	2.34×10^{-4}	5.465×10^{3}	2.454×10^{0}	5.39×10^{-4}	2.166×10^{3}	2.690×10^{0}	1.31×10^{-3}	8.080×10^{2}	2.960×10^{0}
0.030	2.08×10^{-3}	4.375×10^{2}	3.449×10^{0}	4.76×10^{-3}	1.646×10^{2}	4.005×10^{0}	1.15×10^{-2}	5.677×10^{1}	4.823×10^{0}
0.050	5.71×10^{-3}	1.284×10^{2}	4.282×10^{0}	1.30×10^{-2}	4.626×10^{1}	5.228×10^{0}	3.09×10^{-2}	1.478×10^{1}	6.876×10^{0}
0.080	1.44×10^{-2}	3.957×10^{1}	5.531×10^{0}	3.23×10^{-2}	1.338×10^{1}	7.264×10^{0}	7.54×10^{-2}	3.779×10^{0}	1.102×10^{1}
0.100	2.21×10^{-2}	2.209×10^{1}	6.421×10^{0}	4.95×10^{-2}	7.159×10^{0}	8.862×10^{0}	0.114	1.842×10^{0}	1.497×10^{1}
0.150	4.82×10^{-2}	7.226×10^{0}	9.012×10^{0}	0.106	2.090×10^{0}	1.420×10^{1}	0.235	4.038×10^{-1}	3.315×10^{1}
0.200	8.29×10^{-2}	3.059×10^{0}	1.238×10^{1}	0.178	7.777×10^{-1}	2.263×10^{1}	0.379	1.011×10^{-1}	8.208×10^{1}
0.250	0.125	1.482×10^{0}	1.694×10^{1}	0.264	3.241×10^{-1}	3.678×10^{1}	—	—	—
0.300	0.174	7.763×10^{-1}	2.327×10^{1}	0.357	1.417×10^{-1}	6.201×10^{1}	0.678	4.205×10^{-3}	1.102×10^{3}
0.330	—	—	—	—	—	—	0.757	1.097×10^{-3}	3.781×10^{3}
0.350	0.228	4.263×10^{-1}	3.232×10^{1}	0.457	6.240×10^{-2}	1.103×10^{2}	0.805	3.442×10^{-4}	1.134×10^{4}
0.370	—	—	—	—	—	—	0.846	7.038×10^{-5}	5.274×10^{4}
0.380	—	—	—	—	—	—	0.865	2.310×10^{-5}	1.573×10^{5}
0.400	0.286	2.404×10^{-1}	4.561×10^{1}	0.557	2.672×10^{-2}	2.111×10^{2}	—	—	—
0.450	0.348	1.372×10^{-1}	6.577×10^{1}	0.655	1.074×10^{-2}	4.463×10^{2}	—	—	—
0.500	0.412	7.818×10^{-2}	9.748×10^{1}	0.748	3.864×10^{-3}	1.087×10^{3}	—	—	—
0.550	—	—	—	0.831	1.150×10^{-3}	3.289×10^{3}	—	—	—
0.600	0.543	2.414×10^{-2}	2.398×10^{2}	0.901	2.397×10^{-4}	1.455×10^{4}	—	—	—
0.650	—	—	—	0.954	2.158×10^{-5}	1.527×10^{5}	—	—	—
0.700	0.669	6.329×10^{-3}	7.415×10^{2}	—	—	—	—	—	—
0.800	0.784	1.151×10^{-3}	3.481×10^{3}	—	—	—	—	—	—
0.900	0.878	7.947×10^{-5}	4.505×10^{4}	—	—	—	—	—	—
0.950	0.914	6.283×10^{-6}	5.471×10^{5}	—	—	—	—	—	—
0.980	0.932	2.387×10^{-7}	1.412×10^{7}	—	—	—	—	—	—
0.990	0.937	2.057×10^{-8}	1.630×10^{8}	—	—	—	—	—	—

TABLE 4. Permeability k/a^2 and resistance force per unit length $F/\mu U$ for cubic lattices of circular fibres as a function of fibre radius a with solid volume fraction ϕ. All results are accurate to within ±1 in the last figure. (*a*) SC lattice (*b*) BCC lattice, (*c*) FCC lattice.

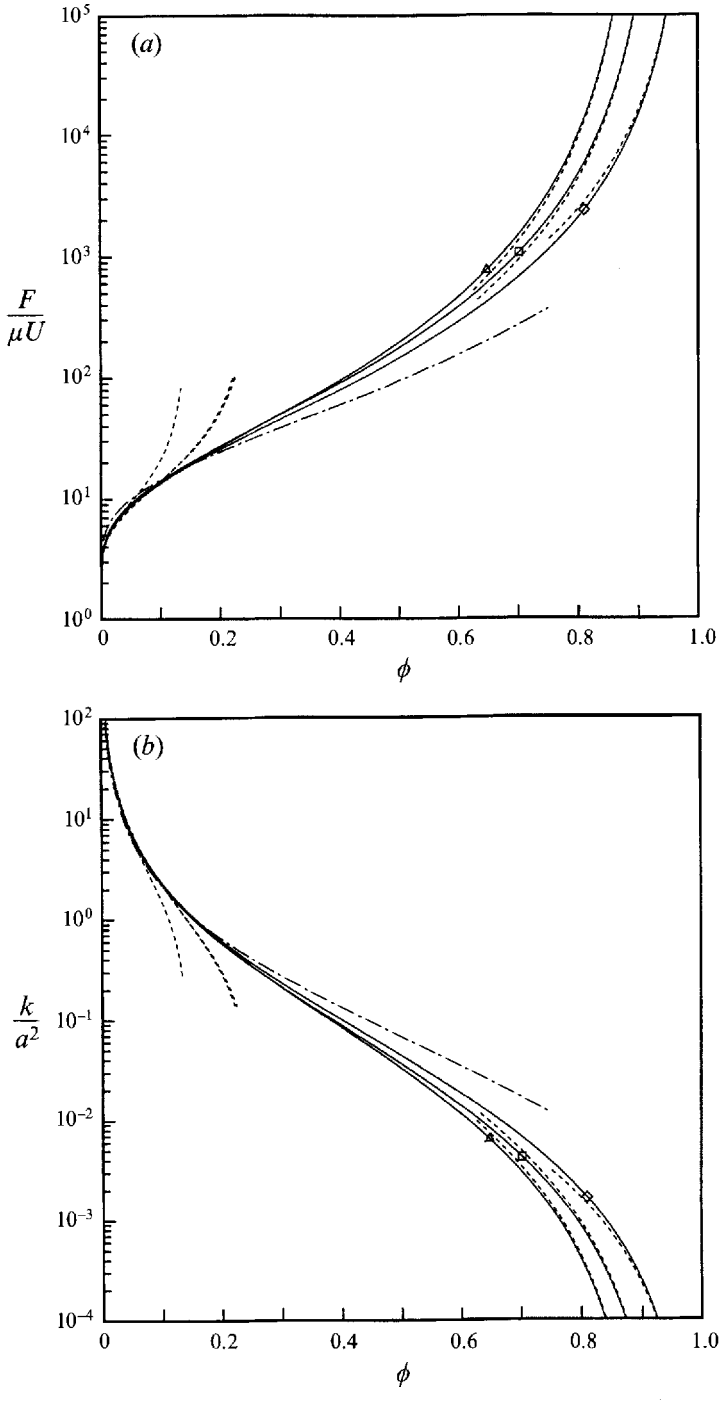

FIGURE 4. (*a*) Resistance force per unit length $F/\mu U$ and (*b*) permeability k/a^2 for fibrous media as a function of solid volume fraction ϕ. Solid lines are computed results for three-dimensional cubic lattices: □, SC; ◇, BCC; △, FCC; dashed curves are asymptotic results from slender-body theory and lubrication theory; dashed-dotted line is the model of Jackson & James, equation (27).

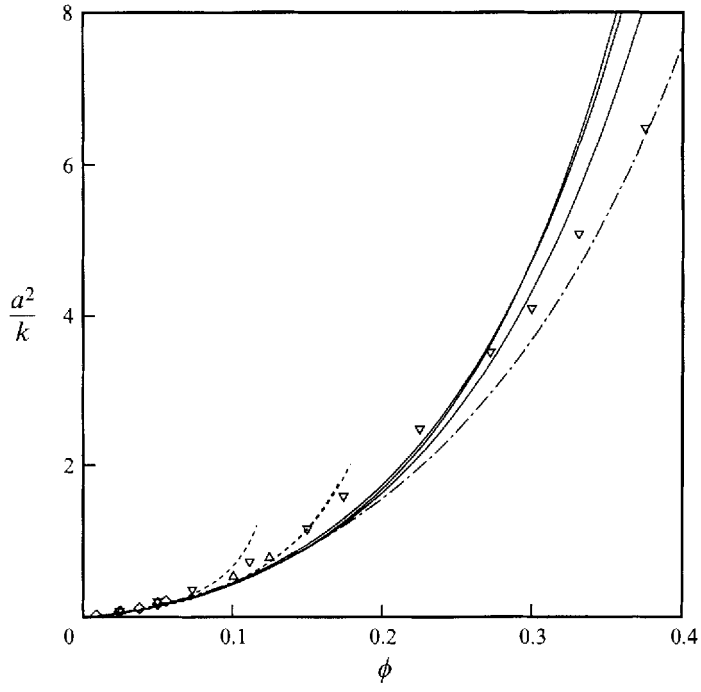

FIGURE 5. Resistivity a^2/k for fibrous media plotted as a function of solid volume fraction ϕ. Solid lines are computed results for three-dimensional cubic lattices. Open symbols are results of Claeys & Brady (1993*b*) for dispersions of prolate spheroids: $\diamond$, $d/a = 20$; $\triangle$, $d/a = 10$; $\triangledown$, $d/a = 6$. Dashed–dotted line is the model of Jackson & James, equation (27).

would expect given the simple relationship (20) between F and k. It is interesting to observe that the FCC medium has the lowest permeability of the three cubic lattices. This reflects the fact that, in some sense, the FCC lattices distribute the fibres in a more uniform manner throughout the volume. It is well known (Jackson & James 1986) that a non-uniform distribution of material yields a higher permeability owing to the disproportionate flow increase in the less-dense regions.

In our final figure, we compare the present results with those of Claeys & Brady (1993*a–c*) for disordered dispersions of prolate spheroids. Following those authors, we plot the resistivity of the medium (a^2/k) as a function of volume fraction in figure 5. This figure includes results for spheroids of aspect ratio 6, 10 and 20. For non-interacting particles in the dilute limit, the resistivity is directly proportional to ϕ with only a logarithmic dependence on aspect ratio. This explains the nearly linear behaviour from a volume fraction of 0 to approximately 5%. The departure from linearity at higher ϕ is associated with the particle interactions. The spheroids with aspect ratios of 10 and 20 show good agreement with the ordered lattices for all data reported by Claeys & Brady, including volumes fractions up to approximately 12%. The shorter particles with aspect ratio 6 begin to show departures from the fibre lattice results, yet even these particles show reasonable agreement up to volume fractions of 30%. (For these higher concentrations, Claeys & Brady observed a nematic phase transition and reported separate resistivities for the two principal directions. Here we show the results averaged over all orientations.) Both the ordered lattices of this paper and the disordered dispersions of Claeys & Brady fall within the scatter of the experimental data reported by Jackson & James and represented by their model equation (27).

In this paper, our primary concern has been the behaviour of fibrous media at finite values of ϕ. From the discussion above, we observe that the ordered fibre lattices and disordered dispersions show little difference in macroscopic properties at these volume fractions. It is important to emphasize however that the limiting values for dilute systems may show significant differences owing to the difference between the continuous fibrous medium and the dispersed spheroidal suspensions. As the volume fraction of the fibre lattice approaches zero, the fibre radius approaches zero, while the length remains constant. Thus the aspect ratio d/a approaches infinity as $\phi^{-1/2}$. The fibres maintain a continuous connected solid phase with $O(1)$ interactions in the neighbourhood of the fibre junctions. This regime where $\phi\, d^2/a^2$ is $O(1)$ is characterized as a semi-dilute system. The asymptotic form of the resistivity is

$$a^2/k \sim \phi \ln \phi^{-1/2} + O(\phi/(\ln \phi^{-1/2})^2),$$

as may be inferred directly from the slender body result (37) with $d/a \sim \phi^{-1/2}$. Dispersed suspensions in the semi-dilute regime will show the same leading term, but the first correction may take a different form dependent upon the structure of the suspension. By contrast, for dispersed suspensions of particles with fixed aspect ratio d/a, all interactions approach zero as $\phi \to 0$, and the suspension falls within the dilute regime. The scaling of the resistivity is similar to that for dilute suspensions of spheres, i.e. $\phi/\ln(d/a) + O(\phi^{4/3})$ for periodic systems and $\phi/\ln(d/a) + O(\phi^{3/2})$ for random systems (Howells 1974). Thus the resistivity results of Claeys & Brady will show significant differences from the present model at infinitesimal values of ϕ. The ratio of the resistivity in the two systems will scale as $\ln \phi^{-1/2}/\ln d/a$. The reader is referred to the papers of Clays & Brady (1993*a–c*) for a further discussion of the transport properties of dispersed suspensions.

In this paper, we have computed the resistance force F and permeability k for ordered fibrous media based on SC, BCC and FCC cubic lattices. We have presented accurate numerical results for the full range of volume fractions, and we have developed analytical estimates based on the limiting asymptotic theories. We have compared our results with simple models based on two-dimensional media, and with numerical simulations for disordered suspensions. All of these results are found to be consistent with the widely scattered experimental observations.

This work was supported by the National Science Foundation and the Petroleum Research Fund administered by the American Chemical Society. Gregory D. Ford acknowledges the support of the Department of Energy through a Computational Science Graduate Fellowship.

REFERENCES

CHAPMAN, A. M. & HIGDON, J. J. L. 1992 Oscillatory Stokes flow in periodic porous media. *Phys. Fluids* A **4**, 2099–2116.

CHAPMAN, A. M. & HIGDON, J. J. L. 1994 Effective elastic properties for a periodic bicontinuous porous medium. *J. Mech. Phys. Solids* **42**, 283–305.

CLAEYS, I. L. & BRADY, J. F. 1993*a* Suspensions of prolate spheroids in Stokes flow. Part 1. Dynamics of a finite number of particles in a unbounded fluid. *J. Fluid Mech.* **251**, 441–442.

CLAEYS, I. L. & BRADY, J. F. 1993*b* Suspensions of prolate spheroids in Stokes flow. Part 2. Statistically homogeneous dispersions. *J. Fluid Mech.* **251**, 443–477.

CLAEYS, I. L. & BRADY, J. F. 1993*c* Suspensions of prolate spheroids in Stokes flow. Part 3. Hydrodynamic transport properties of crystalline dispersions. *J. Fluid Mech.* **251**, 411–442.

DRUMMOND, J. E. & TAHIR, M. I. 1984 Laminar viscous flow through regular arrays of parallel solid cylinders. *Intl J. Multiphase Flow* **10**, 515–540.

HASIMOTO, H. 1959 On the periodic fundamental solutions of the Stokes equations and their application to viscous flow past a cubic array of spheres. *J. Fluid Mech.* **5**, 174–177.

HOWELLS, I. D. 1974 Drag due to the motion of a Newtonian fluid through a sparse random array of small fixed rigid objects. *J. Fluid Mech.* **64**, 449–475.

JACKSON, G. W. & JAMES, D. F. 1982 The hydrodynamic resistance of hyaluronic acid and its contribution to tissue permeability. *Biorheology* **19**, 317–330.

JACKSON, G. W. & JAMES, D. F. 1986 The permeability of fibrous porous media. *Can. J. Chem. Engng* **64**, 364–374.

JOHNSON, R. E. 1980 An improved slender-body theory for Stokes flow. *J. Fluid Mech.* **99**, 411–431.

KIM, S. & KARRILA, S. J. 1991 *Microhydrodynamics: Principles and Selected Applications*, Butterworth-Heinemann.

LARSON, R. E. & HIGDON, J. J. L. 1986 Microscopic flow near the surface of two-dimensional porous media. Part 1. Axial flow. *J. Fluid Mech.* **166**, 449–472.

LARSON, R. E. & HIGDON, J. J. L. 1987 Microscopic flow near the surface of two-dimensional porous media. Part 2. Transverse flow. *J. Fluid Mech.* **178**, 119–136.

LARSON, R. E. & HIGDON, J. J. L. 1989 A periodic grain consolidation model of porous media. *Phys. Fluids* A **1**, 38–46.

MULDOWNEY, G. P. & HIGDON, J. J. L. 1995 A spectral boundary element approach to three dimensional Stokes flow. *J. Fluid Mech.* **298**, 167–192.

POZRIKIDIS, C. 1992 *Boundary and Singularity Methods for Linearized Viscous Flow*. Cambridge University Press.

SANGANI, A. S. & ACRIVOS, A. 1982*a* Slow flow past periodic arrays of cylinders with application to heat transfer. *Intl J. Multiphase Flow* **8**, 193–206.

SANGANI, A. S. & ACRIVOS, A. 1982*b* Slow flow through a periodic array of spheres. *Intl J. Multiphase Flow* **8**, 343–360.

SANGANI, A. S. & YAO, C. 1988*a* Transport processes in random arrays of cylinders. I. Thermal conduction. *Phys. Fluids* **31**, 2426–2434.

SANGANI, A. S. & YAO, C. 1988*b* Transport processes in random arrays of cylinders. II. Viscous flow. *Phys. Fluids* **31**, 2426–2434.

SPARROW, E. M. & LOEFFLER, A. L. 1959 Longitudinal laminar flow between cylinders arranged in a regular array. *AIChE J.* **5**, 325–330.

SPIELMAN, L. & GOREN, S. L. 1968 Model for predicting pressure drop and filtration efficiency in fibrous media. *Environ. Sci. Technol.* **2**, 279–287.

VAN DYKE, M. 1974 Analysis and improvement of perturbation series. *Q. J. Mech. Appl. Maths* **27**, 423–450.

ZICK, A. A. & HOMSY, G. M. 1982 Stokes flow through periodic arrays of spheres. *J. Fluid Mech.* **115**, 13–26.